UHASSELT
KNOWLEDGE IN ACTION

Maastricht University

Faculty of Medicine and Life Sciences
School for Life Sciences
Master of Biomedical Sciences

Master's thesis

Transient Receptor Potential Vanilloid 4 inhibition regulates microglial cytoskeleton dynamics in vitro

Nathan Stas

Thesis presented in fulfillment of the requirements for the degree of Master of Biomedical Sciences, specialization Molecular Mechanisms in Health and Disease

SUPERVISOR :

Prof. dr. Bert BRONE

MENTOR :

dr. Yeranddy AGUIAR ALPIZAR

2020
2021

Transnational University Limburg is a unique collaboration of two universities in two countries: the University of Hasselt and Maastricht University.

UHASSELT
KNOWLEDGE IN ACTION

www.uhasselt.be
Universiteit Hasselt
Campus Hasselt:
Martelarenlaan 42 | 3500 Hasselt
Campus Diepenbeek:
Agoralaan Gebouw D | 3590 Diepenbeek

UHASSELT
KNOWLEDGE IN ACTION

Maastricht University

Faculty of Medicine and Life Sciences
School for Life Sciences
Master of Biomedical Sciences

Master's thesis

Transient Receptor Potential Vanilloid 4 inhibition regulates microglial cytoskeleton dynamics in vitro

Nathan Stas

Thesis presented in fulfillment of the requirements for the degree of Master of Biomedical Sciences, specialization Molecular Mechanisms in Health and Disease

SUPERVISOR :

Prof. dr. Bert BRONE

MENTOR :

dr. Yeranddy AGUIAR ALPIZAR

Transient Receptor Potential Vanilloid 4 inhibition regulates microglial cytoskeleton dynamics *in vitro**

Nathan Stas[1], Jolien Beeken[2,3], Bert Brône[3] and Yeranddy A. Alpizar[3]

[1]Biomedical Sciences, Faculty of Medicine and Life Sciences, Universiteit Hasselt, Campus Diepenbeek, Agoralaan Gebouw D – B-3590 Diepenbeek, Belgium
[2]Molecular Regulation of Neurogenesis, GIGA-Stem cells, Université de Liège, Quartier Hôpital, Avenue Hippocrate 15, B-4000 Liège, Belgium
[3]Neurosciences research group, Biomedical Research Institute, Universiteit Hasselt, Campus Diepenbeek, Agoralaan Gebouw C - B-3590 Diepenbeek, Belgium

*Running title: *TRPV4 regulates microglial cytoskeleton*

To whom correspondence should be addressed: Bert Brône, Tel: +32 (11) 26 92 37; Email: bert.brone@uhasselt.be

Keywords: TRPV4; microglia; motility; calcium; cytoskeleton

ABSTRACT

Ramified microglia use their branches to actively scan the healthy central nervous system, a process regulated by intracellular calcium fluctuations. It has been demonstrated that local calcium increases can be initiated by both chemoattractant signal transduction and membrane tension, posing the mechanosensitive members of the Transient Receptor Potential (TRP) superfamily of cation channels as potential transducers of mechanical force into intracellular calcium fluctuations. Indeed, it has recently been shown that the calcium permeable and mechanosensitive channel TRP Vanilloid 4 (TRPV4) contributes to microglial motility. However, it is still unknown how TRPV4 regulates the microglial cytoskeleton. Using high-end live microscopy techniques, this study showed that inhibition of TRPV4 decreases actin and tubulin cytoskeleton dynamics of cultured primary mouse microglia. Furthermore, inhibition resulted in loss of their extensive ramifications. Hereby, this study suggests that TRPV4 is crucial for proper microglial motility and surveillance of the central nervous system.

INTRODUCTION

Microglia are essential to maintain proper development and homeostasis of the central nervous system (CNS). For instance, they eliminate excess synapses during development and sense danger signals during adult life. Therefore, these macrophage-like cells have been termed the innate immune cells of the CNS. Depending on the health status and region of the CNS, together with the age and sex of the organism, microglia can obtain a spectrum of morphologies ranging from ramified to ameboid. A ramified 'resting' morphology is characterized by a small soma and multiple long thin branched processes, whereas an ameboid 'active' morphology is defined by a round soma and very few thick, short processes (1). Although ramified microglia have initially been termed as resting, research has shown that these microglia actively extend and retract their branches to scan their environment (2, 3). This process, termed motility, is used in the healthy adult CNS to monitor possible homeostatic changes. In contrast, migration is defined as the active movement of the soma that occurs when microglia sense potential threats and adapt an ameboid morphology to attempt elimination of these threats by moving to the affected area (1). While it has been challenging to study ramified microglia *in vitro* due to the rapid adaptation of an ameboid morphology directly after isolation, a recent study determined transforming growth factor-β2 (TGF-β2), interleukin 34 (IL-34), and cholesterol as crucial factors in the culture medium of primary isolated microglia. Consequently, this study was able to reproduce microglia *in vitro* with a morphology similar to that

of mature ramified microglia *in vivo* (4).

A recent *in vivo* study investigated microglial calcium (Ca^{2+}) signaling in awake mice using two-photon microscopy. This study revealed that microglial processes exhibit very low and infrequent Ca^{2+} signaling during basal conditions. In contrast, the processes respond to changes in neuronal activity through increased Ca^{2+} signaling, resulting in process extension (5). Earlier work already established that both motility and migration depend on the surrounding extracellular matrix (ECM) of the microglia. More specifically, the movement of the soma and branches is accomplished via orchestrated assembly and disassembly of cytoskeletal protein complexes that attach to the ECM. These protein complexes are termed focal adhesions and are formed by activated integrins, transmembrane receptors composed of non-covalently linked α and β subunits (1). It has been demonstrated in migrating cells *in vitro* that the assembly and disassembly of focal adhesions are regulated by Ca^{2+} signaling, more specifically intracellular Ca^{2+} gradients and local Ca^{2+} increases (6, 7). An increase in intracellular Ca^{2+} can originate from intracellular stores (e.g., endoplasmic reticulum) and the extracellular environment of the microglia. The latter is regulated by store-operated Ca^{2+}-permeable channels (e.g., ionotropic purinergic P2X7 receptor) (8). Interestingly, a study in human umbilical vein endothelial cells demonstrated that inhibiting Ca^{2+} release from the endoplasmic reticulum by blocking receptor tyrosine kinase and subsequent production of inositol-1,4,5-triphosphate by phospholipase C simply reduces local Ca^{2+} increases (9). In contrast, removal of extracellular Ca^{2+} completely inhibits Ca^{2+} fluctuations in human fibroblasts. Additionally, this study showed that local Ca^{2+} increases are not only initiated by chemoattractant signal transduction, as described above, but also by membrane tension via a Ca^{2+}-permeable stretch-activated member of the Transient Receptor Potential (TRP) superfamily of ion channels, namely TRPM7 (6). This mechanosensitive character of TRP channels indicates they could be transducers of mechanical force into chemical messengers, more specifically intracellular Ca^{2+} fluctuations.

The TRP superfamily is a family of mostly non-selective cation channels subdivided into seven subfamilies, more particularly canonical (TRPC), vanilloid (TRPV), melastatin (TRPM), polycystin (TRPP), mucolipin (TRPML), ankyrin (TRPA), and NOMPC-like (TRPN) channels. With exception of TRPN channels which are only found in invertebrates and fish, the distribution of these channels is widely spread throughout cell and tissue types. Consequently, they are involved in a variety of physiological processes such as nociception, proprioception, and thermosensation (10, 11). It has been suggested that most members of the TRP family are mechanically gated channels that undergo conformational changes in response to tension imposed on the lipid bilayer, even if the initial stimulus is not mechanical force but, for example, a change in temperature (11). Several Ca^{2+}-permeable TRP channels have been reported to play a role in regulating microglial functions, more specifically TRPC1 (12), TRPC3 (13), TRPM2 (14, 15), TRPM7 (16), TRPV1 (17), TRPV2 (18), and TRPV4 (19).

Interestingly, TRPV4 has been found to regulate the cytoskeleton of migrating cells both dependent and independent of Ca^{2+}. Research in endometrial cancer cells demonstrated that TRPV4-mediated Ca^{2+}-influxes activate the RhoA/ROCK1 pathway, which in turn causes cytoskeletal rearrangement through upregulation of F-actin and paxillin. The latter is an actin-binding protein that strengthens focal adhesions (20). In contrast, a study in rat dorsal root ganglion neurons and F11 cells showed that the C-terminus of TRPV4 directly interacts with the actin and tubulin cytoskeleton components of the cells, whether Ca^{2+} is present or not. Moreover, this study found that TRPV4 activation resulted in formation of elongated filopodia, structures composed of actin, and the disassembly of microtubules, structures composed of tubulin. The latter was reversed upon administration of Taxol, a microtubule stabilizer that apparently also inhibited TRPV4-mediated Ca^{2+}-influxes (21). Taken together with proof that TRPV4 is activated via mechanical strain in the backbone of the focal adhesion induced by tensional forces applied to β1-integrin in bovine capillary endothelial cells (22), it can be suggested that TRPV4 is present in the focal adhesion complex of microglia and participates in their cytoskeletal rearrangement. Consequently, TRPV4 could contribute to both motility and migration of microglia. Indeed, a recent study in mouse retinal microglia indicated that microglial signaling and

morphology are regulated via TRPV4-mediated Ca^{2+} signaling in response to hypoosmotic conditions, requiring intermediary activation of phospholipase A2, cytochrome P450, and epoxyeicosatrienoic acid production (23). Another recent study showed that the temperature-dependent movement of mouse microglia is regulated by TRPV4 both *in vitro* and *in vivo* (24).

However, it is unknown how TRPV4 regulates the microglial cytoskeleton. This study hypothesized that both pharmacological and genetic inhibition of TRPV4-mediated Ca^{2+}-influxes reduce the cytoskeleton dynamics of ramified mouse microglia *in vitro*. To investigate this, the actin and tubulin dynamics between wild-type and TRPV4-inhibited primary mouse microglia were compared using live imaging techniques. First, this study demonstrated that functional TRPV4 channels are expressed in the soma, lamellipodia, and branches of primary mouse microglia. Moreover, it indicated that microglial morphology, tubulin dynamics, and filopodia motility are dependent on TRPV4 activity. These results are important since identification of the mechanisms responsible for proper microglial surveillance may contribute to the development of therapeutic interventions for neurological diseases caused by microglial dysfunction.

EXPERIMENTAL PROCEDURES

Reagents – All reagents were purchased at Sigma-Aldrich (Darmstadt, Germany) unless stated otherwise.

Animals – *Trpv4*$^{-/-}$ mice were kindly provided by the Laboratory for ion channel research at KU Leuven. $CX_3CR_1^{eGFP/eGFP}$ mice were obtained from the European Mouse Mutant Archive with approval of (25). An in-house breeding provided post-natal day 21 (P21) $CX_3CR_1^{eGFP/-}$*Trpv4*$^{-/-}$ mouse pups and their wild type (WT) littermates ($CX_3CR_1^{eGFP/-}$*Trpv4*$^{+/+}$) from a C57BL/6J background. In exception, $CX_3CR_1^{-/-}$ mice were used for live Ca^{2+} imaging. Animals were housed on a 12 h light/dark cycle in standard facilities with access to food and water *ad libitum*. Experiments were approved by the institutional Ethics Committee for Animal Welfare.

Genotyping – Mice were genotyped using the KAPA Mouse Genotyping Kit. DNA extraction was performed at 75 °C for 15 min using extraction buffer (2% 1 U/µl KAPA Express Extract Enzyme, 10% 10X KAPA Express Extract Buffer, 88% Milli-Q). One microliter sample (diluted 1:2) was added to the PCR mix solution (52% 2X KAPA2G Fast Genotyping Mix, 32.29% Milli-Q, 5.25% of each primer). Primer sequences used were 5'-CAT GAA ATC TGA CCT CTT GTC CCC-3' (*Trpv4*$^{-/-}$ forward), 5'-CTG TCC CAG CCT CCC CTC CT-3' (*Trpv4*$^{+/+}$ forward), and 5'-GCT CCT GTT GAA CAT GCT TAT CG-3' (reverse) (IDT, Coralville, IA, United States). The PCR program performed was 1 x 3 min at 95 °C, 40 x 15 sec at 95 °C + 15 sec at 65 °C + 1 min at 72 °C, 1 x 1 min at 72 °C, and held at 4 °C. Samples were loaded on an agarose gel (2% agarose (Invitrogen, Thermo Fisher Scientific, Waltham, MA, United States), 1X TAE, 1:10 000 GelRed (Biotium, Hayward, CA, United States)) together with the 100 bp DNA SmartLadder (Eurogentec, Liège, Belgium). Voltage was established at 160 V for 1 h and the gel was read using D-DiGit gel scanner (LI-COR Biosciences, Lincoln, NE, United States).

Primary microglia isolation – Cortical $CD11b^+$ cells were isolated using magnetic activated cell sorting (MACS) following a protocol adapted from (26). Briefly, P21 brains were isolated and placed in ice-cold HBSS (Gibco, Thermo Fisher Scientific) to aid removal of the meningeal layer. Brains were washed in high-glucose DMEM supplemented with 1% Penicillin/Streptomycin (P/S, Lonza, Basel, Switzerland) and vigorous pipetting was executed to disintegrate the tissue. Next, the tissue was incubated with papain (17 U/mg) and DNase I (Roche, Basel, Switzerland) for 30 min at 37 °C. The single cell suspension was filtered using a 70 µm cell strainer, centrifuged (500 x g, 5 min), and gently resuspended in 30% stock isotonic percoll (GE Healthcare, Chicago, IL, United States) (SIP) solution. A 70% SIP solution was pipetted underneath to create a gradient. This gradient was topped with PBS 1X and centrifuged (650 x g, 25 min, brake 0). Afterwards, mono-nuclear cells were isolated, diluted with PBS 1X, and centrifuged (500 x g, 5 min, 4 °C). $CD11b^+$ cells were isolated using MACS CD11b MicroBeads, OCTOMacs separator, and MS columns (Miltenyi Biotec, Bergisch Gladbach,

Germany) according to manufacturer's instructions. Resulting $CD11b^+$ cells were seeded in 10:10:1 medium (10% foetal calf serum, 10% horse serum, 1% P/S in high-glucose DMEM) onto glass coverslips (30 x 10^3 cells/ml), 24-well plates (30 x 10^3 cells/ml), or 35 mm MatTek glass bottom dishes (10 x 10^4 cells/ml, MatTek, Ashland, MA, United States) coated with Poly-D Lysine (20 µg/ml, Gibco) and Collagen type IV (2 µg/ml), and incubated in a humified incubator at 37 °C, 8.5% CO_2.

Cell culture optimization – $CD11b^+$ cells were cultured in a 24-well plate for 7 days before cell medium was refreshed or changed to DMEM/F12 (Gibco) or medium optimized by (4) (TIC, 5 µg/ml Insulin, 5 µg/ml N-Acetyl-Cysteine, 100 µg/ml Apo-transferrin, 0.1 µg/ml Na^+-Selenite, 1 µg/ml Heparan Sulfate, 2 µg/ml Human TGF-β2 (PeproTech, Rocky Hill, NJ, United States), 0.1 µg/ml Murine IL-34 (BioLegend, San Diego, CA, United States), 1.5 µg/ml Ovine Wool Cholesterol, 3 µg/ml L-glutamine in DMEM/F12). After 5 days, cells were imaged using the Incucyte S3 (Essen BioScience, Ann Arbor, MI, United States) and analysed using Fiji (27) by manually defining cell contours and quantifying shape parameters. The optimized protocol consisted of 7 days 10:10:1 medium followed by 3-5 days TIC medium and was used throughout the rest of the study.

Morphology – $CD11b^+$ cells cultured in a 24-well plate were treated with 1 µM or 10 µM GSK2193874 (Tocris Bioscience, Bristol, United Kingdom) and imaged for 48 h with the Incucyte S3. All images were analysed using Fiji by manually defining cell contours and quantifying shape parameters at different time points.

Live Ca^{2+} and tubulin imaging – $CD11b^+$ cells cultured in 24-well glass bottom plates (Ibidi, Gräfelfing, Germany) or glass bottom dishes were incubated with Fluo-4 AM (2 µM, Invitrogen) or SiR-Tubulin (0.05 nM, Spirochrome, Stein am Rhein, Switzerland) for respectively 30 min and 1 h at 37 °C. Afterwards, cells were imaged during a time series before and/or after being exposed to solutions containing GSK2193874 (10 µM), GSK1016790A (300 nM, Tocris Bioscience), Yoda-1 (50 µM, Tocris Bioscience) and/or ATP (10 µM) prepared in standard Krebs (150 mM NaCl, 6 mM KCl, 10 mM HEPES, 10 mM glucose, 1.5 mM $CaCl_2$, 1 mM $MgCl_2$, pH 7.4) or Ca^{2+}-free Krebs (150 mM NaCl, 6 mM KCl, 10 mM HEPES, 10 mM Glucose, 2 mM EDTA, 1 mM $MgCl_2$, pH 7.4) either manually or via perfusion by gravity using a multi-barrelled pipette tip. Live Ca^{2+} images were obtained with the 10X objective and analysed using Fiji by manually selecting subcellular regions and measuring fluorescent intensity. All values were normalized, and maximum amplitudes were calculated in Microsoft Excel version 16.48 (21041102) for MacOS (Microsoft, Redmond, WA, United States). Live tubulin images were obtained with the 100X oil objective followed by structured illumination microscopy processing on the Zeiss Elyra (Carl Zeiss AG, Oberkochen, Germany) and analysed using the PIVlab toolbox (28) in MATLAB release 2021a (9.10.0.1649659) (MathWorks, Natick, MA, United States).

(High-resolution) confocal microscopy – **TRPV4 and F-actin staining.** $CD11b^+$ cells cultured on glass coverslips were incubated with ice-cold fixation buffer (4% paraformaldehyde, 0.3% Triton X-100, 5% sucrose in PBS 1X) for 15 min at room temperature (RT), washed with washing buffer (0.2% Triton X-100 in PBS 1X), and incubated with blocking buffer (5% bovine serum albumin, 0.3% Tween-20, 0.2% Triton X-100 in PBS 1X) overnight at 4 °C. Afterwards, cells were incubated with primary antibody against TRPV4 (1:200, Alomone Labs, Jerusalem, Israel) overnight at 4 °C, washed with washing buffer, and incubated with goat anti-rabbit Alexa Fluor 647 (1:600, Life Technologies, Thermo Fischer Scientific) and Alexa Fluor 594 Phalloidin (1:40, Invitrogen) for 1 h at RT. Finally, cells were washed with washing buffer, incubated with DAPI (1:10 000) for 15 min at RT, and mounted onto glass slides using Fluoromount-G (Invitrogen). Alternatively, cells were directly mounted using the DAPI-containing mounting solution VectaShield (Vector Laboratories, Burlingame, CA, United States). Confocal images were obtained using the optimal pinhole size for the 63X objective on the Zeiss LSM 880-Airyscan (Carl Zeiss AG) and processed in Fiji. **Filopodia motility.** $CD11b^+$ cells were cultured in a 24-well glass bottom plate and imaged during a time series before and after exposure to a GSK2193874 (10 µM) solution prepared in standard Krebs. Confocal images were

obtained using the optimal pinhole size for the 63X oil objective on the Zeiss LSM 880-Airyscan. All images were analysed using Fiji by manually defining cell contours and quantifying shape parameters and area (fraction).

Quantitative real-time PCR – RNA was isolated from cell pellets using the RNeasy Mini Kit (Qiagen, Hilden, Germany) following manufacturer's instructions. Purity and concentration were assessed with the NanoDrop 2000 (Thermo Fisher Scientific). cDNA was synthesized using reverse transcription with the qScript cDNA SuperMix (VWR, Radnor, PA, United States) and diluted to a final concentration of 5 ng/µl. Real-time PCR was performed on the StepOnePlus Real-Time PCR system (Applied Biosystems, Foster City, CA, Unites States) using the SYBR Green Master Mix (Applied Biosystems), probes for *Trpv4*, *Trpm7*, *Piezo1*, *Piezo2* and *Gapdh* (IDT) and the following program: 1 x 20 sec at 95 °C, 40 x 3 sec at 95 °C + 30 sec at 60 °C, 1 x 15 sec at 95 °C + 1 min at 60 °C + 15 sec at 95 °C. Results were analysed in Microsoft Excel via the comparative C_T method ($\Delta\Delta C_T$).

Statistical analysis – Data was statistically analysed using GraphPad prism version 9.1.0 (216) for MacOS (GraphPad Software, La Jolla, CA, United States) using the appropriate parametric or non-parametric test as indicated in the figure legends. Normality was assessed using the Shapiro-Wilk test.

RESULTS

TGF-β2, IL-34, and cholesterol in culture medium increase microglial ramifications – Prior to commencing the experiments, it was important to determine the culture medium in which microglia best develop a ramified morphology. To achieve this, isolated *Trpv4*$^{+/+}$ microglia were cultured in high-glucose basal medium (10:10:1), serum-free medium (DMEM/F12), or serum-free medium supplemented with, most importantly, human TGF-β2, murine IL-34, and ovine wool cholesterol (TIC). The latter is based on a previous medium optimization by Bohlen *et al.* (4). Microglia cultured in 10:10:1 medium appeared to have a small and elongated morphology with pronounced

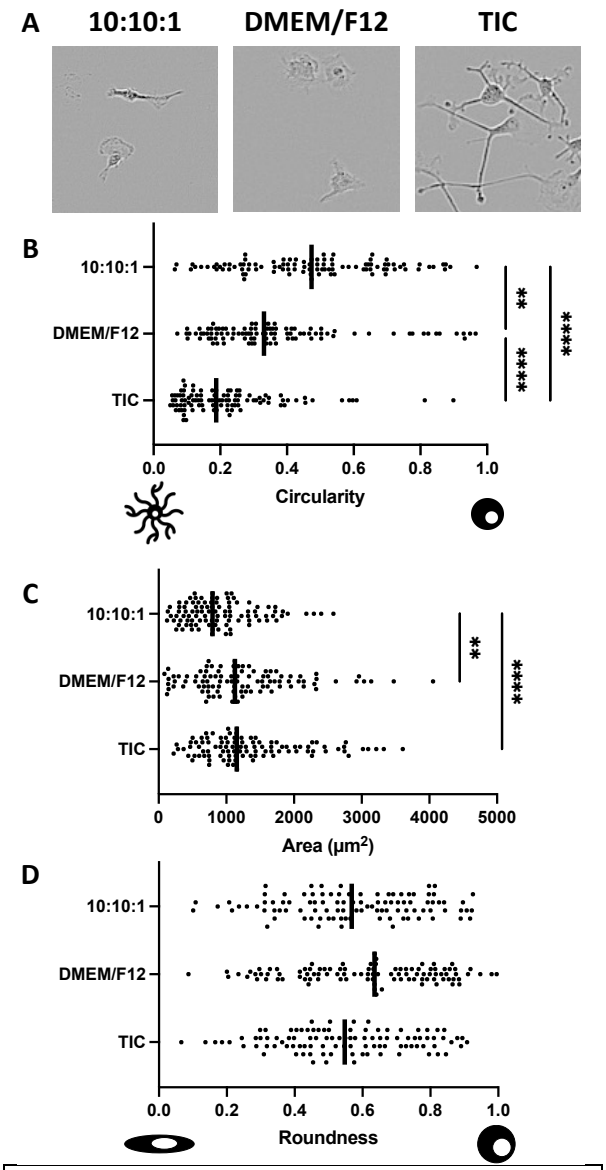

Figure 1: TIC medium decreases microglial circularity. Representative images **(A)** and median circularity **(B)**, area **(C)**, and roundness **(D)** of *Trpv4*$^{+/+}$ microglia cultured in high-glucose basal medium (10:10:1), serum-free medium (DMEM/F12), or optimized TIC medium. **p<0.01; ****p<0.0001. Kruskal-Wallis test with Dunn's multiple comparison. n=100 per condition.

lamellipodia **(Figure 1A)**. Quantitative morphological analysis showed that these microglia had a median circularity of 0.474 **(Figure 1B)** and a median area of 797.13 µm^2 **(Figure 1C)**. In contrast, microglia cultured in DMEM/F12 and TIC

medium appeared to have a larger and more ramified morphology **(Figure 1A)**. Indeed, quantification demonstrated that microglia cultured in serum-free DMEM/F12 had a significantly lower circularity (median of 0.331, $p<0.01$) and bigger area (median of 1126.85 μm^2, $p<0.01$) compared to those cultured in 10:10:1 medium. Moreover, those cultured in TIC medium displayed an even greater decrease in circularity (median of 0.188, $p<0.0001$) and increase in area (median of 1155.15 μm^2, $p<0.0001$) **(Figure 1B,C)**. The culture medium had no effect on roundness of the microglia **(Figure 1D)**. From this data it could be concluded that TIC medium is the preferred medium for culturing isolated microglia throughout this study.

TRPV4 is functionally expressed in cortical microglia – To assess the subcellular protein expression of TRPV4 and its colocalization with the microglial cytoskeleton, *Trpv4*$^{+/+}$ microglia were stained for TRPV4 and F-actin. High resolution confocal images showed that TRPV4 is expressed in the soma **(Figure 2A,C)**, branches **(Figure 2B)**, and lamellipodia **(Figure 2D)** of *Trpv4*$^{+/+}$ microglia.

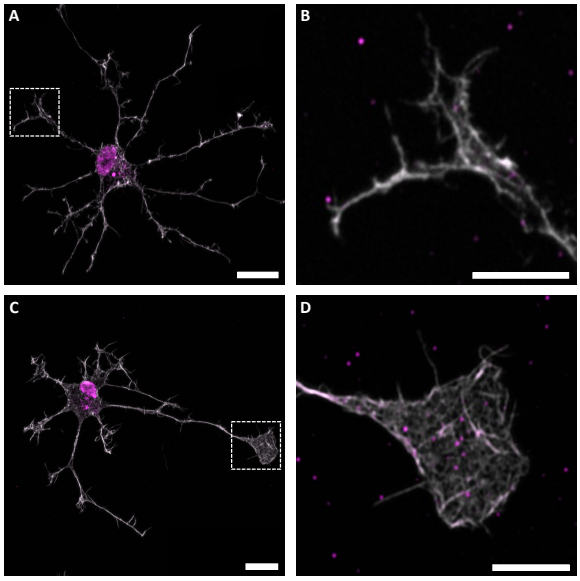

Figure 2: TRPV4 protein is expressed in the soma, branches, and lamellipodia of microglia. High-resolution confocal images of *Trpv4*$^{+/+}$ microglia stained for TRPV4 (magenta) and F-actin (white). Whole-cell images **(A,C)** with inserts of a branch **(B)** and lamellipodium **(D).** Scale bars: 10 µm (A,C) and 5 µm (B,D).

In addition to protein expression, functional TRPV4 expression was examined in the different subcellular regions. To achieve this, the cell permeable fluorescent Ca^{2+} indicator Fluo-4 was utilized to compare Ca^{2+} fluctuations in *Trpv4*$^{+/+}$ and *Trpv4*$^{-/-}$ microglia in response to TRPV4 agonist GSK1016790A (300 nM). The agonist was able to trigger Ca^{2+} fluctuations in all regions of *Trpv4*$^{+/+}$ microglia that were reversible upon washout **(Figure 3A,B)**. In contrast, it was largely unable to elicit a response in Ca^{2+}-free conditions, when TRPV4 antagonist GSK2193874 (10 µM) was present, or in *Trpv4*$^{-/-}$ microglia **(Figure 3C,D)**. This demonstrates that functional TRPV4 channels are expressed in all subcellular regions of cortical microglia.

TRPV4 inhibition reduces microglial tubulin dynamics – To investigate the effect of TRPV4 inhibition on the microglial tubulin structures, the cell permeable fluorescent dye SiR-Tubulin was used to stain the microtubules of untreated *Trpv4*$^{+/+}$ microglia, *Trpv4*$^{+/+}$ microglia treated with TRPV4 antagonist GSK2193874 (10 µM), and *Trpv4*$^{-/-}$ microglia. Microscopic images indicated that untreated *Trpv4*$^{+/+}$ microglia have highly motile microtubules **(Figure 4A)**. This was confirmed when quantification of the movement showed a median vector velocity of 0.6123 µm/min **(Figure 4B,C)**. In contrast, there was a significant decrease in vector velocity in both GSK2193874 treated *Trpv4*$^{+/+}$ (median of 0.3757 µm/min, $p<0.0001$) and *Trpv4*$^{-/-}$ (median of 0.4373 µm/min, $p<0.0001$) microglia **(Figure 4B,C)**. Moreover, the sum of all vector velocities per interrogation region and the median vector velocity per timepoint were also significantly decreased in GSK2193874 treated *Trpv4*$^{+/+}$ (median of 5.5 µm/min, $p<0.0001$ and median of 0.3571 µm/min, $p<0.0001$) and *Trpv4*$^{-/-}$ (median of 6.963 µm/min, $p<0.0001$ and median of 0.4875 µm/min, $p<0.05$) microglia compared to untreated *Trpv4*$^{+/+}$ microglia (median of 8.439 µm/min and 0.5705 µm/min) **(Figure 4D,E)**. These results demonstrate that both pharmacological and genetic inhibition of TRPV4 decrease the tubulin dynamics of microglia.

TRPV4 inhibition reduces microglial actin dynamics – Additionally, the filopodia of *Trpv4*$^{+/+}$ microglia were imaged before and after treatment with TRPV4 antagonist GSK2193874 (10 µM)

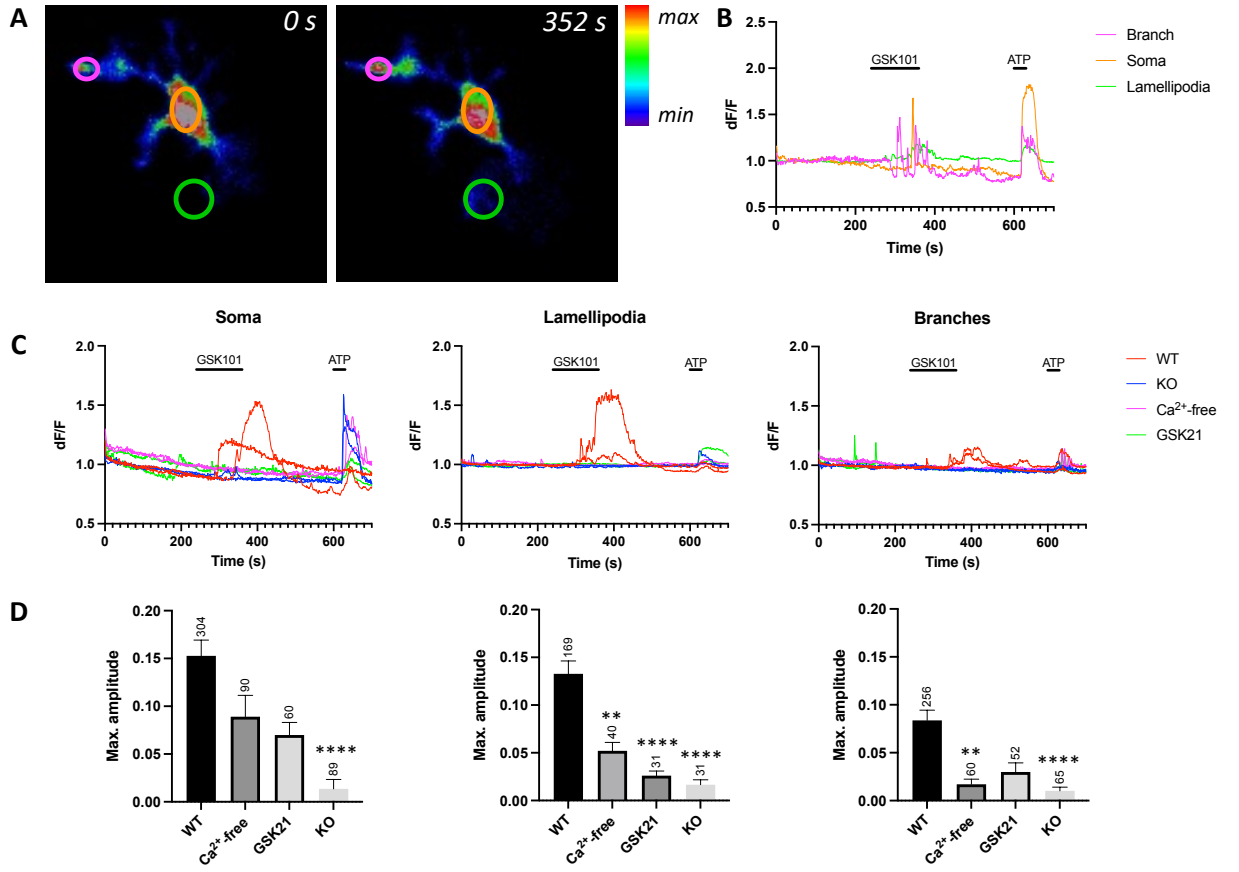

Figure 3: TRPV4 is functionally expressed in microglia. Representative microscopic images **(A)** and Ca^{2+} traces per region **(B)** of a *Trpv4*$^{+/+}$ microglia showing increased Ca^{2+} fluctuations in the presence of GSK1016790A (300 nM). Representative Ca^{2+} traces **(C)** and maximum amplitudes of Ca^{2+} fluctuations in response to GSK1016790A (300 nM) **(D)** recorded in WT (*Trpv4*$^{+/+}$), Ca^{2+}-free, GSK2193874 (10 µM), and KO (*Trpv4*$^{-/-}$) conditions. ATP (10 µM) was applied at the end to assess cellular responsiveness. Data shown as mean ± SEM. Scale bar: 10 µm. **p<0.01; ****p<0.0001. Kruskal-Wallis test with Dunn's multiple comparison.

(Figure 5A). Because filopodia are actin structures (29), this would determine the effect of acute TRPV4 inhibition on microglial actin dynamics. High-resolution confocal images indicated that filopodia in *Trpv4*$^{+/+}$ microglia are highly dynamic **(Figure 5B)**. Over a timespan of three minutes, these filopodia scanned an area of 46.54 ± 4.442 µm^2. Moreover, *Trpv4*$^{+/+}$ microglia have a high number of filopodia (35.26 ± 1.826) with substantial length (1.957 ± 0.035 µm) **(Figure 5D,E)**. In contrast, filopodia in TRPV4-inhibited microglia scanned significantly less area (33.11 ± 3.438 µm^2, p<0.0001) **(Figure 5C)**. Moreover, the number and length of filopodia were significantly lower after acute inhibition of TRPV4 (26.53 ± 1.9 and 1.509 ± 0.034, p<0.0001) **(Figure 5D,E)**. Combined, this data suggests that acute TRPV4 inhibition decreases the filopodia and thus actin dynamics of microglia.

Microglial morphology is dependent on TRPV4 – Next, *Trpv4*$^{+/+}$ microglia were treated with TRPV4 antagonist GSK2193874 (1 µM and 10 µM) for 48 h to further investigate the effect of reduced cytoskeleton dynamics on microglial morphology. Whereas untreated microglia did not change in morphology over time, both concentrations of the inhibitor caused the microglia to retract their branches and obtain a rounded morphology **(Figure 6A)**. Quantification showed that microglia treated with 10 µM GSK2193874 already had a significant increase in circularity at

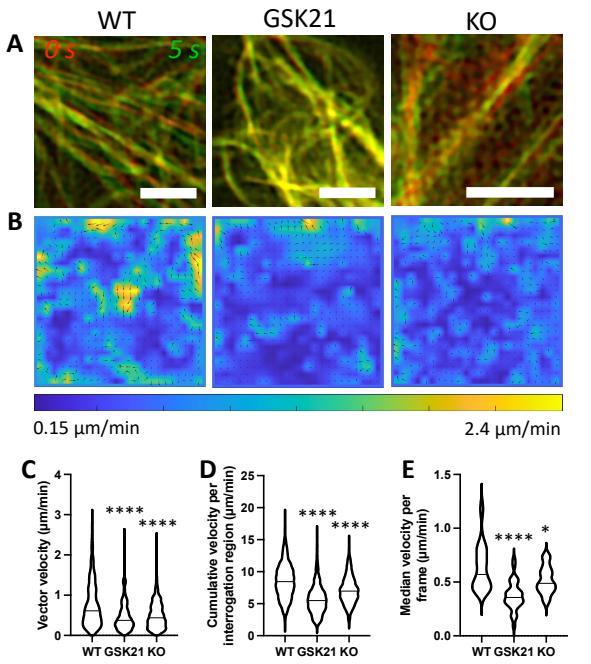

Figure 4: Microglial tubulin dynamics decrease by both pharmacologic and genetic TRPV4 inhibition. Representative microscopic images **(A)**, heatmap **(B)**, and velocity **(C)** of tubulin structures recorded in WT (*Trpv4*$^{+/+}$), GSK2193874 (10 µM), and KO (*Trpv4*$^{-/-}$) conditions. Cumulative velocity per interrogation region for the duration of 1 min **(D)** and median velocity per frame for the duration of 30 s **(E)** of tubulin structures recorded in WT (*Trpv4*$^{+/+}$), GSK2193874 (10 µM), and KO (*Trpv4*$^{-/-}$) conditions. Scale bar: 2 µm. *p<0.05; ****p<0.0001. Mann-Whitney test. n=5 per condition.

30 min (0.340 ± 0.022, p<0.001), and that they reached a 67.06% increase at 48 h (0.568 ± 0.028, p<0.0001). In contrast, microglia treated with 1 µM GSK2193874 only reached a significant increase at 48 h (116.33%, 0.424 ± 0.037, p<0.0001) **(Figure 6B)**. Moreover, microglia treated with both 1 µM and 10 µM GSK2193874 already had a significantly decreased area at 30 min (1186.576 ± 71.317, p<0.01 and 637.566 ± 34.269, p<0.0001) and reached a 58.94% and 35.77% decrease in area at 48 h (487.198 ± 44.039, p<0.0001 and 409.505 ± 22.035, p<0.0001), respectively **(Figure 6B)**. However, the TRPV4 antagonist had no effect on roundness of the microglia **(Figure 6B)**. Thus, it can be concluded that TRPV4 regulates the morphology of ramified microglia.

In an independent experiment, *Trpv4*$^{+/+}$ and *Trpv4*$^{-/-}$ microglia were cultured in 10:10:1 medium and treated with TRPV4 antagonist GSK2193874 (10 µM) for 24 h to assess possible off-target effects. There was no significant difference in microglial morphology at baseline between both conditions when untreated **(Figure 6C)**. Furthermore, comparing the morphological effects of the antagonist between *Trpv4*$^{+/+}$ and *Trpv4*$^{-/-}$ microglia excluded the possibility of off-target effects **(Figure 6D)**.

Genetic inhibition of TRPV4 does not cause upregulation of Trpm7, Piezo1, and Piezo2 – To investigate possible compensatory mechanisms in *Trpv4*$^{-/-}$ microglia, a quantitative PCR was performed to compare gene expression levels of several known mechanosensitive Ca^{2+} permeable channels, namely *Trpm7*, *Piezo1*, and *Piezo2* (6, 30). The gene expression levels of all three genes were similar in *Trpv4*$^{+/+}$ microglia, with *Piezo2* having the highest expression level. When comparing the gene expression with *Trpv4*$^{-/-}$ microglia, no significant differences were found, although *Piezo2* seemed to be less expressed **(Figure 7A)**. The similar expression level of *Piezo1* was confirmed when its agonist Yoda-1 (50 µM) was able to trigger Ca^{2+} fluctuations in both *Trpv4*$^{+/+}$ and *Trpv4*$^{-/-}$ microglia with similar amplitudes **(Figure 7B,C)**. There was thus no sign that *Trpv4*$^{-/-}$ microglia upregulate *Trpm7*, *Piezo1* or *Piezo2* as compensatory mechanisms for the constitutive lack of functional TRPV4.

DISCUSSION

This study aimed to investigate how the Ca^{2+}-permeable and mechanosensitive cation channel TRPV4 regulates the cytoskeleton of primary mouse microglia *in vitro*. The results showed that TRPV4 inhibition reduces both the tubulin and actin dynamics of the microglial cytoskeleton. Furthermore, they demonstrated that TRPV4 inhibition induces acute changes on the morphology of ramified microglia. Taken together, these results suggest that TRPV4 regulates the morphology of microglia by contributing to the movement of their actin and tubulin cytoskeleton.

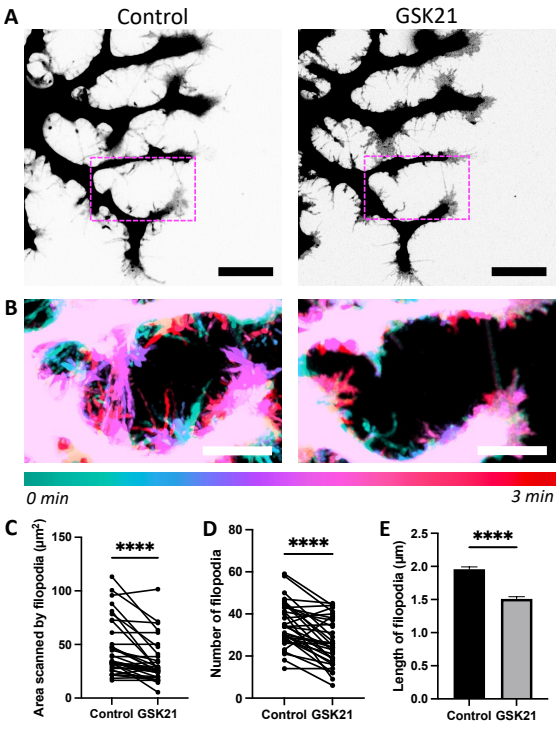

Figure 5: Acute TRPV4 inhibition reduces movement, number, and length of microglial filopodia. Representative high-resolution confocal images **(A)** and temporal color-coded inserts **(B)** of *Trpv4*$^{+/+}$ microglia untreated and treated with GSK2193874 (10 µM). Scanned area **(C)**, number **(D)**, and length **(E)** of filopodia of *Trpv4*$^{+/+}$ microglia untreated and treated with GSK2193874 (10 µM). Data shown as mean ± SEM. Scale bars: 10 µm (A), 5 µm (C). ****p<0.0001. C: Wilcoxon signed rank test. D: Paired t-test. E: Mann-Whitney test. n=7.

First and foremost, the research presented here supports the recent discovery that TGF-β2, IL-34, and cholesterol are crucial factors for the development of mature ramified microglia, which will aid future *in vitro* microglial research (4). Furthermore, it demonstrated that functional TRPV4 channels are expressed in microglia, which is in line with previous reports in both resting and activated microglia (19, 23, 24).

Pharmacologic and genetic inhibition of TRPV4 both caused a significant decrease in tubulin dynamics. However, only pharmacologic inhibition induced acute changes in microglial morphology, resulting in smaller microglia that lost their ramifications. This indicates existence of compensatory mechanisms in *Trpv4*$^{-/-}$ microglia that allow them to obtain a proper ramified morphology. Still, these compensatory mechanisms are not able to fully compensate for the loss of TRPV4, as indicated by the decreased tubulin dynamics in *Trpv4*$^{-/-}$ microglia. This demonstrates that TRPV4 is crucial for proper microglial surveillance, which is supported by a recent *in vivo* study that showed decreased surveillance by TRPV4-inhibited microglia. Interestingly, this study also revealed that *Trpv4*$^{-/-}$ microglia do have a different morphology from *Trpv4*$^{+/+}$ microglia, characterized by shorter branches and less branching points (31). The contrast with the morphological findings in this study can possibly be explained by studying microglia *in vitro* versus *in vivo*, as the latter allows for the more complex Sholl analysis to quantify morphological characteristics of cells. Nevertheless, this report further strengthens the findings of this study and supports the idea that TRPV4 is crucial for proper microglial morphology and surveillance.

The current study investigated several Ca^{2+}-permeable and mechanosensitive channels that could be upregulated in *Trpv4*$^{-/-}$ microglia as compensatory mechanisms for the constitutive lack of functional TRPV4. These channels included TRPM7, Piezo1, and Piezo2. Unexpectedly, *Trpv4*$^{-/-}$ microglia did not upregulate the gene expression levels of these channels. This does not, however, eliminate the possibility that these channels are compensatory mechanisms, nor does it eliminate the possibility that other compensatory mechanisms are present in *Trpv4*$^{-/-}$ microglia. A single-cell RNA sequencing should be executed to evaluate the differences between *Trpv4*$^{+/+}$ and *Trpv4*$^{-/-}$ microglia.

The simultaneous assembly of focal adhesions at the leading edge and disassembly at the rear end allows for movement of the branches and/or displacement of the soma, and both are influenced by changes in the local microenvironment of the microglia, neuronal activity in the brain, and signal molecules secreted by surrounding cells (1). Several proteins involved in this Ca^{2+}-dependent control of the microglial cytoskeleton have been discovered in migrating cells. For instance, a study in human umbilical vein endothelial cells has found that local Ca^{2+} increases at the leading edge activate myosin light-chain kinase and myosin II, which in

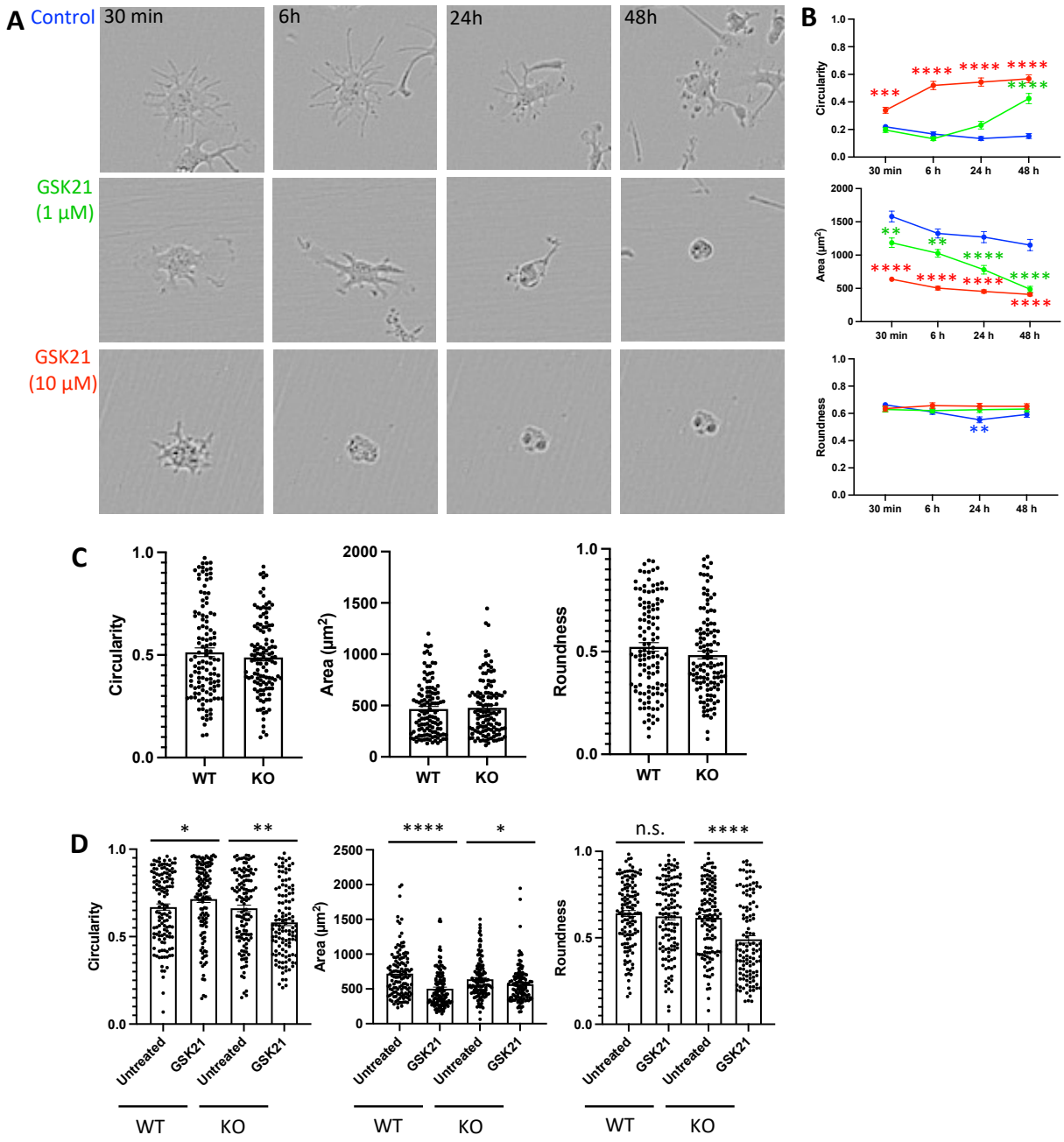

Figure 6: Acute TRPV4 inhibition changes microglial morphology. Representative images **(A)** and mean circularity, area, and roundness **(B)** of *Trpv4*$^{+/+}$ microglia untreated and treated with GSK2193874 (1 µM and 10 µM) for 48 h. Mean circularity, area, and roundness of WT (*Trpv4*$^{+/+}$) and KO (*Trpv4*$^{-/-}$) microglia untreated **(C)** and treated with GSK2193874 (10 µM) for 24 h **(D)**. Data shown as mean ± SEM. *p<0.05; **p<0.01; ***p<0.001; ****p<0.0001. A,B: Kruskal-Wallis test with Dunn's multiple comparison, n=100 per condition; C,D: Mann-Whitney test, n≥118 per condition.

turn trigger contraction of actin filaments. The force generated by myosin II causes both retraction of the protruding lamellipodium and recruitment of paxillin to the focal adhesion to strengthen the complex (7). In contrast, calpain, a Ca^{2+}-dependent cysteine protease, has been found to cleave components of the focal adhesion complex in response to elevated Ca^{2+}, causing it to disassemble

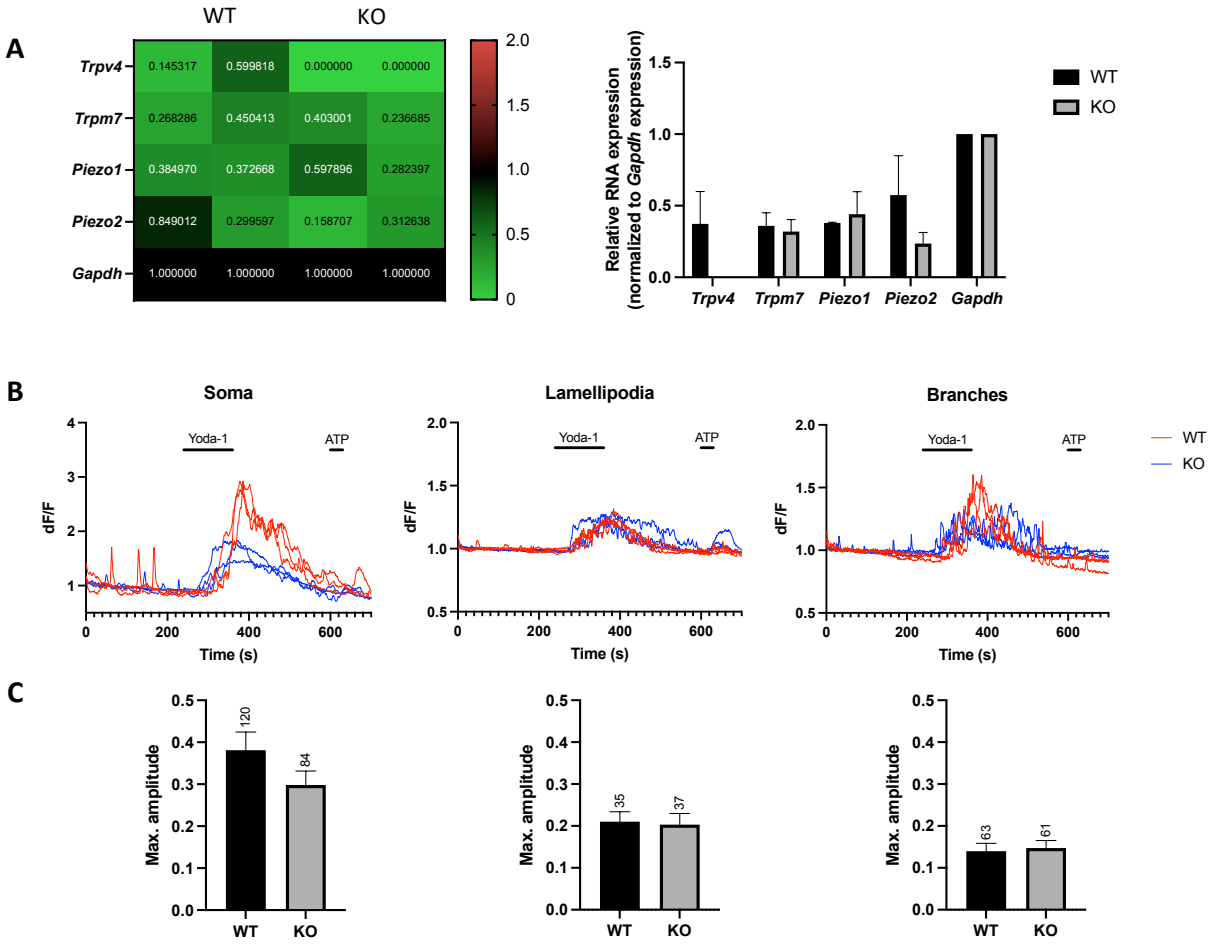

Figure 7: Mechanosensitive Ca^{2+} permeable channels TRPM7, Piezo1, and Piezo2 are not upregulated in *Trpv4*$^{-/-}$ microglia. Heatmap and bar graph **(A)** of a quantitative real-time PCR for *Trpv4*, *Trpm7*, *Piezo1*, and *Piezo2* normalized to *Gapdh* expression. n=2. Representative Ca^{2+} traces **(B)** and maximum amplitudes **(C)** of Ca^{2+} fluctuations in response to Piezo1 agonist Yoda-1 (50 µM) recorded in WT (*Trpv4*$^{+/+}$) and KO (*Trpv4*$^{+/+}$) conditions. ATP (10 µM) was applied at the end to assess cellular responsiveness. Data shown as mean ± SEM.

(32). As a result, it can be suggested that TRPV4-mediated Ca^{2+}-influxes play a role in these processes by upregulating the proteins necessary to assemble and disassemble focal adhesions, which has previously been shown in trabecular meshwork cells in the eye (33). However, earlier work in other migrating cells already demonstrated that TRPV4 can regulate the cytoskeleton both dependently and independently of Ca^{2+}, for instance through its C-terminus (20, 21). Future studies should thus investigate both the Ca^{2+}-dependent and Ca^{2+}-independent mechanisms through which TRPV4 regulates the microglial actin and tubulin cytoskeleton. The former can be achieved by pull down assays, whereas simultaneously live imaging Ca^{2+} and cytoskeleton dynamics can investigate the latter.

Additionally, it would be interesting to visualize the colocalization of TRPV4 within the focal adhesion complex, which can consist of over 100 different proteins (34). As previously mentioned, focal adhesions are formed by activated integrins, and this activation can occur through both intracellular and extracellular signaling. The former requires binding of cytoskeletal proteins (e.g., talin) to the cytoplasmic tail of the β subunit, whereas the latter requires binding of an ECM ligand (e.g., collagen) to the extracellular head of the integrin (35). Both will induce recruitment of actin-binding proteins such as paxillin to the complex, allowing

for the formation of mature focal adhesions. Thus, co-staining TRPV4 with focal adhesion proteins such as integrin β1, talin, and paxillin would be interesting.

This research had few minor limitations. Throughout the experiments, collagen type IV was used to coat the surface onto which freshly isolated $CD11b^+$ cells were seeded, mainly due to its beneficial effect on the adhesion, survival, and ramifications of microglia (4). While collagen type IV is (highly) expressed in the basement membrane of the ECM in the CNS, its expression level in the interstitial matrix, where microglia reside, is quite low. Future *in vitro* studies should consider using highly expressed interstitial matrix proteins, for example fibronectin or vitronectin (1). Additionally, this study investigated the live motility of filopodia as a method for studying actin dynamics. While filopodia are actin structures and therefore a good model for this experiment (29), it would be more compelling to use a live F-actin dye in future studies to visualize the dynamics of the individual actin filaments.

CONCLUSION

This study revealed that the mechanosensitive Ca^{2+} permeable channel TRPV4 contributes to the regulation of the actin and tubulin cytoskeleton in primary mouse microglia. As a result, TRPV4 controls microglial morphology. The significance of this research is substantial, as it implicates that TRPV4 is a crucial factor for proper microglial motility and consequently microglial surveillance of the CNS. Accordingly, the insights presented in this study may contribute to the development of therapies for disorders caused by microglial dysfunction.

REFERENCES

1. Smolders SM-T, Kessels S, Vangansewinkel T, Rigo J-M, Legendre P, Brône B. Microglia: Brain cells on the move. Progress in Neurobiology. 2019;178:101612.
2. Davalos D, Grutzendler J, Yang G, Kim JV, Zuo Y, Jung S, et al. ATP mediates rapid microglial response to local brain injury in vivo. Nature Neuroscience. 2005;8(6):752-8.
3. Nimmerjahn A, Kirchhoff F, Helmchen F. Resting microglial cells are highly dynamic surveillants of brain parenchyma in vivo. Science. 2005;308(5726):1314-8.
4. Bohlen CJ, Bennett FC, Tucker AF, Collins HY, Mulinyawe SB, Barres BA. Diverse Requirements for Microglial Survival, Specification, and Function Revealed by Defined-Medium Cultures. Neuron. 2017;94(4):759-73.e8.
5. Umpierre AD, Bystrom LL, Ying Y, Liu YU, Worrell G, Wu LJ. Microglial calcium signaling is attuned to neuronal activity in awake mice. Elife. 2020;9.
6. Wei C, Wang X, Chen M, Ouyang K, Song LS, Cheng H. Calcium flickers steer cell migration. Nature. 2009;457(7231):901-5.
7. Tsai FC, Meyer T. Ca2+ pulses control local cycles of lamellipodia retraction and adhesion along the front of migrating cells. Curr Biol. 2012;22(9):837-42.
8. Kettenmann H, Hanisch UK, Noda M, Verkhratsky A. Physiology of microglia. Physiol Rev. 2011;91(2):461-553.
9. Tsai FC, Seki A, Yang HW, Hayer A, Carrasco S, Malmersjo S, et al. A polarized Ca2+, diacylglycerol and STIM1 signalling system regulates directed cell migration. Nat Cell Biol. 2014;16(2):133-44.
10. Nilius B, Owsianik G. The transient receptor potential family of ion channels. Genome Biol. 2011;12(3):218.
11. Liu C, Montell C. Forcing open TRP channels: Mechanical gating as a unifying activation mechanism. Biochem Biophys Res Commun. 2015;460(1):22-5.
12. Sun Y, Chauhan A, Sukumaran P, Sharma J, Singh BB, Mishra BB. Inhibition of store-operated calcium entry in microglia by helminth factors: implications for immune suppression in neurocysticercosis. J Neuroinflammation. 2014;11:210.
13. Mizoguchi Y, Kato TA, Seki Y, Ohgidani M, Sagata N, Horikawa H, et al. Brain-derived neurotrophic factor (BDNF) induces sustained intracellular Ca2+ elevation through the up-regulation of surface transient receptor potential 3 (TRPC3) channels in rodent microglia. J Biol Chem. 2014;289(26):18549-55.
14. Akyuva Y, Naziroglu M, Yildizhan K. Selenium prevents interferon-gamma induced activation of TRPM2 channel and inhibits inflammation, mitochondrial oxidative stress, and apoptosis in microglia. Metab Brain Dis. 2021;36(2):285-98.
15. Miyake T, Shirakawa H, Kusano A, Sakimoto S, Konno M, Nakagawa T, et al. TRPM2 contributes to LPS/IFNgamma-induced production of nitric oxide via the p38/JNK pathway in microglia. Biochem Biophys Res Commun. 2014;444(2):212-7.
16. Jiang X, Newell EW, Schlichter LC. Regulation of a TRPM7-like current in rat brain microglia. J Biol Chem. 2003;278(44):42867-76.
17. Sappington RM, Calkins DJ. Contribution of TRPV1 to microglia-derived IL-6 and NFkappaB translocation with elevated hydrostatic pressure. Invest Ophthalmol Vis Sci. 2008;49(7):3004-17.
18. Maksoud MJE, Tellios V, An D, Xiang YY, Lu WY. Nitric oxide upregulates microglia phagocytosis and increases transient receptor potential vanilloid type 2 channel expression on the plasma membrane. Glia. 2019;67(12):2294-311.
19. Konno M, Shirakawa H, Iida S, Sakimoto S, Matsutani I, Miyake T, et al. Stimulation of transient receptor potential vanilloid 4 channel suppresses abnormal activation of microglia induced by lipopolysaccharide. Glia. 2012;60(5):761-70.

20. Li X, Cheng Y, Wang Z, Zhou J, Jia Y, He X, et al. Calcium and TRPV4 promote metastasis by regulating cytoskeleton through the RhoA/ROCK1 pathway in endometrial cancer. Cell Death Dis. 2020;11(11):1009.
21. Goswami C, Kuhn J, Heppenstall PA, Hucho T. Importance of non-selective cation channel TRPV4 interaction with cytoskeleton and their reciprocal regulations in cultured cells. PLoS One. 2010;5(7):e11654.
22. Matthews BD, Thodeti CK, Tytell JD, Mammoto A, Overby DR, Ingber DE. Ultra-rapid activation of TRPV4 ion channels by mechanical forces applied to cell surface beta1 integrins. Integr Biol (Camb). 2010;2(9):435-42.
23. Redmon SN, Yarishkin O, Lakk M, Jo A, Mustafic E, Tvrdik P, et al. TRPV4 channels mediate the mechanoresponse in retinal microglia. Glia. 2021;69(6):1563-82.
24. Nishimoto R, Derouiche S, Eto K, Deveci A, Kashio M, Kimori Y, et al. Thermosensitive TRPV4 channels mediate temperature-dependent microglia movement. Proc Natl Acad Sci U S A. 2021;118(17).
25. Jung S, Aliberti J, Graemmel P, Sunshine MJ, Kreutzberg GW, Sher A, et al. Analysis of fractalkine receptor CX(3)CR1 function by targeted deletion and green fluorescent protein reporter gene insertion. Mol Cell Biol. 2000;20(11):4106-14.
26. Stark JC, Wallace E, Lim R, Leaw B. Characterization and Isolation of Mouse Primary Microglia by Density Gradient Centrifugation. J Vis Exp. 2018(132).
27. Schindelin J, Arganda-Carreras I, Frise E, Kaynig V, Longair M, Pietzsch T, et al. Fiji: an open-source platform for biological-image analysis. Nat Methods. 2012;9(7):676-82.
28. Thielicke W, Stamhuis EJ. PIVlab – Towards User-friendly, Affordable and Accurate Digital Particle Image Velocimetry in MATLAB. Journal of open research software. 2014;2(1):e30-e.
29. Gallop JL. Filopodia and their links with membrane traffic and cell adhesion. Semin Cell Dev Biol. 2020;102:81-9.
30. Jiang Y, Yang X, Jiang J, Xiao B. Structural Designs and Mechanogating Mechanisms of the Mechanosensitive Piezo Channels. Trends Biochem Sci. 2021;46(6):472-88.
31. Mertens M, Beeken J, Brône B, Aguiar YA. Microglial branch motility and morphology are regulated by TRPV4 channel [Master thesis]: Hasselt University; 2021.
32. Sackmann E. How actin/myosin crosstalks guide the adhesion, locomotion and polarization of cells. Biochim Biophys Acta. 2015;1853(11 Pt B):3132-42.
33. Lakk M, Krizaj D. TRPV4 - Rho signaling drives cytoskeletal and focal adhesion remodeling in trabecular meshwork cells. Am J Physiol Cell Physiol. 2021.
34. Fraley SI, Feng Y, Krishnamurthy R, Kim DH, Celedon A, Longmore GD, et al. A distinctive role for focal adhesion proteins in three-dimensional cell motility. Nat Cell Biol. 2010;12(6):598-604.
35. Shattil SJ, Kim C, Ginsberg MH. The final steps of integrin activation: the end game. Nat Rev Mol Cell Biol. 2010;11(4):288-300.

Acknowledgements – NS acknowledges the Faculty of Medicine and Life Sciences for his senior internship. NS is grateful for a position in the Neurosciences research group of Prof. Dr. Bert Brône. Melanie Mertens, Rosette Beenaerts and Sofie Kessels are thanked for assisting with experiments. The dynamic bio-imaging lab is thanked for providing access to the Zeiss Elyra and Zeiss LSM 880-Airyscan.

Author contributions – BB and YAA conceived and designed the research. NS, JB and YAA performed experiments and data analysis. NS wrote the paper. All authors carefully edited the manuscript.